IEEE Access
Multidisciplinary | Rapid Review | Open Access Journal

Received 6 January 2023, accepted 16 January 2023, date of publication 18 January 2023, date of current version 26 January 2023.

Digital Object Identifier 10.1109/ACCESS.2023.3237941

SURVEY

Spectrally Efficient Backscatter Systems: A Hardware-Oriented Survey

MOHAMMAD ALHASSOUN, (Member, IEEE)
Department of Electrical Engineering, King Fahd University of Petroleum and Minerals, Dhahran 31261, Saudi Arabia
Center for Communication Systems and Sensing, King Fahd University of Petroleum and Minerals, Dhahran 31261, Saudi Arabia

e-mail: malhassoun@kfupm.edu.sa

This publication is based upon work supported by King Fahd University of Petroleum & Minerals. The author acknowledges the Deanship of Research Oversight and Coordination for the support received under Grant no. SR201011.

ABSTRACT The growing interest in backscatter communications as a low-powered solution in various fields necessitates pushing the envelope of current backscatter systems in multiple frontiers, among which is spectral efficiency. The increase in spectral efficiency can drive real-time applications such as augmented reality. In most of backscatter-system applications such as radio-frequency identification, backscatter modulation is implemented using binary schemes realized with square pulses, which are not spectral efficient. To address the spectral efficiency concern, this article reviews—with a scope limited to *prototyped* systems—some of the existing works in the literature that pertain to increasing the spectral efficiency of backscatter systems. The prototyped systems can be grouped—based on the implementation technique used—into three groups: High-order modulation, single-sideband modulation, and pulse shaping. Based on the current trends and studied literature, the article concludes with discussions on some future directions and open-ended research problems such as optimal pulse shaping, the use of artificial intelligence, multi-carrier modulation, and agile modulation; which are all aim for overcoming the spectral-efficiency limit of contemporary backscatter systems.

INDEX TERMS ASK, backscatter communications, PSK, pulse shaping, QAM, RFID, single sideband modulation.

I. INTRODUCTION

Since its initial proposal [1], backscatter communications (e.g., radio-frequency identification (RFID)[1]) continue to receive growing interest beyond the supply chain industry. With a plethora of applications in various fields such as healthcare [2], crowd management [3], oil and gas industry [4]; the need for a better utilization of the available spectrum is a necessity. This need is not only driven by the massive deployment of backscatter transponders, but also by the requirement to co-exist with non-backscattered systems such as Bluetooth Low Energy (BLE) and WiFi with which the radio spectrum is shared.

Most of the available backscatter systems are in the field of RFID. Therefore, these systems follow Electronic Product Code (EPC) Generation 2 (Gen2) protocol [5],[2] which governs the air interface of RFID systems. This protocol identifies several parameters such frequency, modulation scheme, and bandwidth. These parameters along with others relevant to this article are presented in Subsection II-A. The protocol, although mature, suffers from several limitations that motivate industry and academia to go beyond what Gen2 can offer. An example of such an effort appeared in an academia-industry joint workshop entitled "*What Should Gen3 Be?*" [7].

The associate editor coordinating the review of this manuscript and approving it for publication was Giorgio Montisci.

[1]Throughout this article, the terms backscatter communications and RFID are used interchangeably although backscatter communications include RFID. The rationale behind this use is that the majority of backscatter communications applications are in the field of RFID.

[2]These systems can also follow ISO/IEC 18000-63 standard [6]. However, since this standard is not freely accessible, the analysis in the article assumed Gen 2 protocol.

In Gen2 protocol, binary modulation schemes without a pulse shaping filter are used for both uplink and downlink data communication. The use of binary modulation is driven by the low-powered, low signal-to-noise ratio (SNR) nature of these systems. The low-powered nature is a mere result of moving all of the computational functionalities and power-hungry components away from the transponder (RFID tag) to the interrogator (RFID reader). On the other hand, the low SNR originates from the round-trip nature of these systems along with passivity,[3] which in addition to decreasing the backscattered power, it makes the channel more susceptible to small-scale fading [8], [9], [10].

With binary modulation schemes, the full functionality of backscatter communications is not properly utilized. Therefore, in the high SNR scenarios, the use of binary modulation offers a poor spectral efficiency. The same argument can be applied to rectangular pulses in which a considerable amount of energy is wasted in the form of spurious emission in out-of-band channels. To overcome these limitations, several research articles had implemented more spectrally-efficient backscatter systems.

In this survey, a summary of existing research works that *successfully* increase the spectral efficiency of backscatter systems is presented. Although the research literature has a myriad of proposals focusing on increasing the spectral efficiency, few of these proposals had a working prototype. This article focuses on the last—yet smaller—set of the proposals since hardware limitations and implementation difficulties are usually discussed in these articles.

This article structure is as follows: Section II presents a summary of Gen2 protocol along with the metrics that are usually used to evaluate and compare different designs. Section III covers one technique of increasing the spectral efficiency, which is high-order modulation. The second technique, single-side band (SSB) modulation, is discussed thoroughly in Section IV. The last technique, pulse shaping, is presented in Section V. Finally, this article concludes with a summary and research directions towards increasing the spectral efficiency of backscatter communications. Throughout this review, several acronyms and abbreviations are used, which are listed in Table 1 along with their definitions.

II. PRELIMINARIES

Before discussing existing techniques that increase the spectral efficiency of backscatter systems, some introductory materials are presented. The topics covered in this section are mainly in two areas: Gen2 protocol, a standard used for air interface in RFID systems, and comparison metrics, which allow us to compare and contrast various spectrally-efficient proposals and techniques.

[3]These systems are passive in a sense that their tags do not have radio transmitters.

TABLE 1. The list of abbreviations and acronyms.

Acronym	Definition
ASK	Amplitude shift keying
BER	Bit error rate
BLE	Bluetooth Low Energy
CSI	Channel state information
DSB	Double sideband
EVM	Error vector magnitude
FSK	Frequency shift keying
PAM	Pulse amplitude modulation
PIE	Pulse-interval encoding
PR	Phase reversal
PSK	Phase shift keying
QAM	Quadrature amplitude modulation
RFID	Radio-frequency Identification
RSSI	Received signal strength indicator
SAW	Surface acoustic wave
SNR	Signal-to-noise ratio
SSB	Single sideband
UHF	Ultra high frequency

A. Gen2 PROTOCOL

Gen2 protocol [5] defines the physical and logical requirements for RFID systems operating in the 860–960 MHz frequency band. In this protocol, the tag is passive, which requires that the reader talks first. The tag and reader are not required to simultaneously talk, which makes the communication half duplex. The first release of the protocol was in 2004 and the latest revision was in 2018. An RFID system characterized in Gen2 protocol has two components: Interrogator (reader) and transponder (tag). In terms of frequency band, Gen2 complaint systems operate in the ultra-high frequency (UHF) band (precisely, 860–960 MHz). The channel from the reader to the tag is called the downlink channel while the channel from the tag to the reader is known as the uplink channel.

Two parameters of Gen2 protocol are of particular interest to this survey, which are modulation and data encoding. In the case of the former, the downlink modulation can take one of three variants of amplitude shift keying (ASK); namely, single sideband amplitude shift keying (SSB-ASK), double sideband amplitude shift keying (DSB-ASK), or phase-reversal amplitude shift keying (PR-ASK). However, the tag can implement binary phase-shift keying (BPSK) in addition to ASK.

The downlink and uplink channels use different encoding techniques. In the downlink channel, the reader uses a pulse-interval encoding (PIE) technique in which the duration

of data-0 (T_0) represents the reference time interval. The duration of data-0 ranges from 6.25μs to 25μs. On the other hand, the duration of data-1 (T_1) follows $1.5T_0 \leq T_1 \leq 2.0\ T_0$. Data encoding along with binary modulation result in a downlink bit rate that ranges from 6.7 kbps to 128 kbps assuming equiprobable data. On the tag side, the data encoding techniques are either frequency modulation-0 (FM0) or Miller-modulated subcarrier with 4, 8, or 16 transitions per bit. Depending on the encoding technique, the uplink bit rate ranges from 5 kbps to 640 kbps.

Gen2 protocol does not fully exploit battery-assisted (semi-passive) tags. The use of this type of tags can support better channel coding [11], high-order modulations, pulse shaping, and SSB modulation while maintaining an acceptable SNR with minimal power consumption.

B. COMPARISON METRICS

In the literature, three metrics are used in the characterization of the spectral efficiency, which are bit error rate (BER), error vector magnitude (EVM), and energy efficiency.

1) BER

Bit error rate (BER) is the least common metric in the literature. The computation of the BER depends on the modulation type and order along with the signal-to-noise ratio (SNR) [12]. For a binary phase shift keying (BPSK) in an additive white Gaussian noise (AWGN) channel, the BER is

$$\text{BER} = Q\left(\frac{d}{2\sigma}\right), \tag{1}$$

where d is the distance between the alphabet and $Q(\cdot)$ is complementary distribution function given by [12]

$$Q(x) = \frac{1}{\sqrt{2\pi}} \int_x^\infty e^{-t^2/2}\, dt. \tag{2}$$

To compute the BER from the measured complex voltage at the reader, we can use [13] and [14]

$$\text{BER} = Q\left(\frac{\sqrt{\Delta\sigma_{\text{RCS}}}}{2\sigma}\right) = Q\left(\frac{|V_{\text{state 1}} - V_{\text{state 2}}|}{2\sigma}\right), \tag{3}$$

where $\Delta\sigma_{\text{RCS}}$ is the differential radar cross section (RCS) of the tag, $V_{\text{state 1}}$ and $V_{\text{state 2}}$ are the average voltages corresponding to the modulation states 1 and 2, respectively; σ is the one-dimensional noise variance. The noise power (and hence its variance) are evaluated at the output of the receiver matched filter.

One of the major drawback of this technique is that it assumes that the noise is AWGN, which is not always the case especially near DC in which other noise sources dominate [15]. Therefore, an alternative technique is to send a known sequence and perform a bit-by-bit comparison.

2) EVM

Another common metric for evaluating high-order modulation is the error vector magnitude (EVM), which is defined [16] as

$$\text{EVM} = 100\% \cdot \sqrt{\frac{\sum_{k=1}^{N} |\hat{s}_{k_{\text{ideal}}} - \hat{s}_{k_{\text{sample}}}|^2}{\sum_{k=1}^{N} |\hat{s}_{k_{\text{ideal}}}|^2}}, \tag{4}$$

where N is the number of transmitted symbols, $\hat{s}_{k_{\text{ideal}}}$ is the normalized ideal location of the k^{th} sample, and $\hat{s}_{k_{\text{sample}}}$ is the normalized demodulated k^{th} sample. For AWGN channels, the relationship between EVM and SNR can be found using [17] and [18]

$$\text{EVM} = \sqrt{\frac{1}{\text{SNR}}}. \tag{5}$$

For QAM modulated signals, BER is related to EVM using [18] and [19]

$$P_b = 2\left(1 - \frac{1}{\sqrt{M}}\right) Q\left(\sqrt{\frac{3\log_2 M}{M-1}\frac{1}{\text{EVM}^2 \log_2 M}}\right) \tag{6}$$

Equation (6) is valid for square modulation and when $m = \log_2 M$ is even [19].

3) ENERGY EFFICIENCY

The third metric that appears frequently in the literature of backscatter communications is the energy efficiency. Mathematically, energy efficiency (EE) is defined as [20]

$$\text{EE [bit/Joule]} = \frac{\text{Data rate [bit/s]}}{\text{Energy consumption [Joule/s]}}. \tag{7}$$

Basically, EE states how many bits can be transmitted per unit energy. The driving motive is that we have a unit energy and we want to send as many bits as possible. The situation in backscatter systems is the exact opposite. In fact, energy is scarce and the objective is to send as many bits as possible using the minimal possible energy. Therefore, the majority of backscatter literature —from a hardware perspective—uses the following definition for the energy efficiency[4]

$$\text{Energy Efficiency} = \frac{\text{Energy consumption [Joule/s]}}{\text{Data rate [bit/s]}}, \tag{8}$$

which has a unit of [Joule/bit]. Throughout this paper, the definition in (8) is used unless stated otherwise.

III. HIGH-ORDER MODULATION

As indicated in Section II, RFID systems commonly use binary modulation techniques for both reader-to-tag and tag-to-reader links. Increasing the modulation order would increase the spectral efficiency but consequently increases that BER for a given SNR. To design a high-order backscatter modulator, the impedance of the transponder antenna—as shown in Figure 1—should vary between more than two

[4]To differentiate the definitions, we are spelling the word in the case of (8) and using the abbreviation for (7).

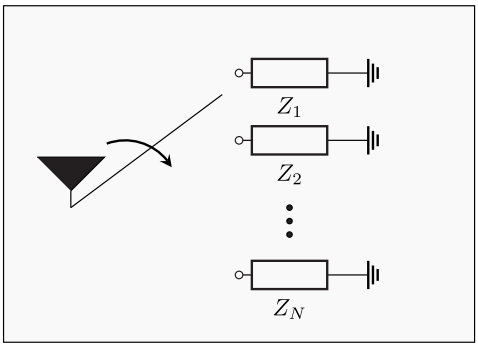

FIGURE 1. A simplified block diagram of a backscatter modulator. $Z_1, Z_2, \ldots, Z_N$ are the load impedances. The switching between impedances takes place in accordance to the sensor data.

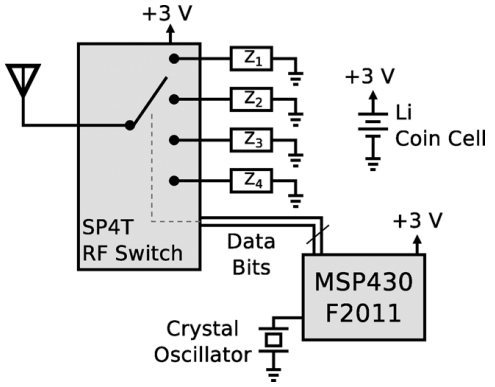

FIGURE 2. A circuit diagram of a 4-PSK/4-QAM backscatter modulator (© 2012 IEEE [21]).

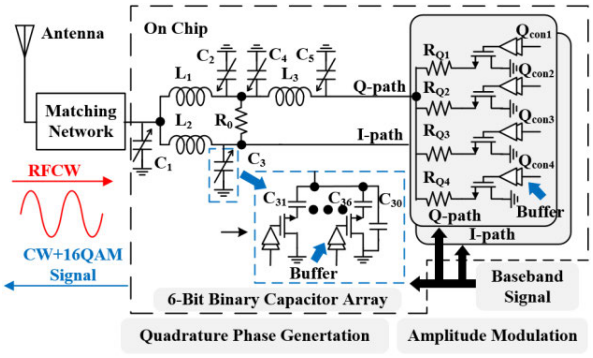

FIGURE 3. The backscatter modulator in [26](© IEEE 2020 [26]).

states in the case of high-order ASK and PSK. However, for a quadrature amplitude modulation (QAM) scheme, another independent channel should be added.

The variation in the antenna impedance can be accomplished using one of three methods:

1) *Lumped elements*. In this case, the antenna is connected to a switch, which in turns connects to discrete resistors, inductors, and/or capacitors.
2) *Delay lines*. In this case, the length of the transmission line is used to synthesize the required impedance.
3) *Solid state*. In this case, the change in biasing voltage of a transistor or a diode changes their impedances. If the antenna is connected to the solid state device, the antenna impedance changes too.

The first and third techniques are more common than the second one since delay lines require increasing the physical dimensions of the backscatter transponder. Furthermore, variation of the impedance using switching circuit offers robustness to the impedance variation with respect to the incident power but at the expense of not having a flexible design. The situation is the exact opposite for a solid-state based impedance variation.

A. LUMPED ELEMENTS

In this case, the impedances in Figure 1 are simply a combination of resistors, capacitors, and/or inductors. The backscatter modulator switches between different impedances. The result is a backscattered field with distinct complex electric field per impedance [22].

1) GENERAL WORK

In the literature, one of the earliest designs was implemented by Thomas et al. [21] (see also [16] for earlier analysis and [23] for a more advanced version) in which a four-state load modulator (shown in Figure 2) is used with all capacitors or combinations of capacitors and inductors. The achieved BER is 10^{-5} in a controlled environment. In order to make the CMOS integration more feasible, Thomas et al. [21] showed that an only resistor-capacitor combination can replace an inductor. The major drawback of this implementation is that the minimum distance between the constellation points is reduced since only the lower half of the Smith chart is used, which in turn results in a high BER. The method of varying the impedance could be also applicable to near-field RFID systems such as [24] and [25].

High-order modulation can be also implemented using a combination of power division and lumped-element terminations. For instance, Gong et al. [26] designed a backscatter tag—shown in Figure 3—implementing a 16-QAM modulation and operating at 2.4 GHz. In the designed tag, three π-type LC networks emulate the performance of a Wilkinson power divider with 90° phase shift. The LC networks modulate the phase of the backscattered signal while the amplitude modulation is accomplished via an array of resistors. The authors in [26] were able to achieve a data rate of 4 Mbps while consuming only 1μW. The overall QAM modulator is fabricated on 0.18μm 1P6M standard CMOS process.

2) APPLICATIONS

In the research literature, several applications and use cases of backscatter communications could benefit from implementing a faster data rate using high-order modulation. One of these applications is ambient backscatter communications [27] in which the source of the incident signal is an ambient source such as an FM radio. As an example, the

throughput of an FM ambient backscatter system can be increased using four frequency-shift keying (4-FSK) modulation scheme, which appears in the work of Wang et al. [28] who developed a backscatter modulator with a bit rate of 3.2 kpbs and an energy efficiency of 3.46 nJ/bit.

WiFi-based ambient backscatter systems are one of the key applications in which high-order modulation can be used. For instance, Kim et al. [29] used four distinct loads (made of lumped elements) to modulate the ambient WiFi signal. In the design of [29], the antenna is connected to four ports with different capacitor values and the change in the capacitor value affects the received signal strength indicator (RSSI) as well as the channel state information (CSI) of the WiFi packet. This change in RSSI and CSI can be detected by a nearby mobile device. Using this technique, the achieved data rate is 60 kbps, which is limited by the duration of a WiFi packet. Another design is proposed by Wang et al. [30] in which the baseband data are mixed with an on-board intermediate frequency (IF) oscillator.[5] In [30], the authors were able to implement a QPSK and achieve a communication range of 91 m. Furthermore, Qian et al. [31] implemented a 4-PSK modulator for ambient tag-to-tag communications.

Current WiFi standards use multi-input multi-output (MIMO) techniques, which results in spatially diverse channels. To exploit this spatial diversity, Zhao et al. [32] designed an ambient system that achieves a throughput of 50 kbps for a single stream and 1 kbps for double streams [32]. A universal version of [32] appeared in the work of Yang and Gong [33] in which any number of streams can be used. In [33], the backscatter modulator can implement PSK (in the work, the authors implemented QPSK) to all OFDM symbols except those in the preamble. In the demodulation stage, the phase pattern in the pilot symbol—which is known to commodity WiFi receivers—is subtracted from the incoming streams. The average phase of all streams is used to estimate the phase of the backscattered signal.

Backscatter communications find also applications in the field of biosensing. For instance, Rosenthal et al. [34] developed a neural recording device (NueroDisc) that uses differential QPSK (DQPSK) (implemented with lumped components) scheme to achieve a rate of 6.25 Mbps with a power consumption of 77.5μW—yielding an energy efficiency of 12.4 pJ/bit. The design in [34] was at UHF frequency band. Other variants of [34] exist such as [35], [36], and [37].

Although the main focus of this work is on radio-based backscatter systems, the use of high-order modulation with a lumped-element modulator recently finds an application in underwater backscatter communications. For instance, Afzal et al. [38] used a piezo-acoustic backscatter system implementing 4-QAM to increase the throughput of underwater backscatter communications.

[5]Elaboration on IF backscatter tags is deferred to the solid-state based designs.

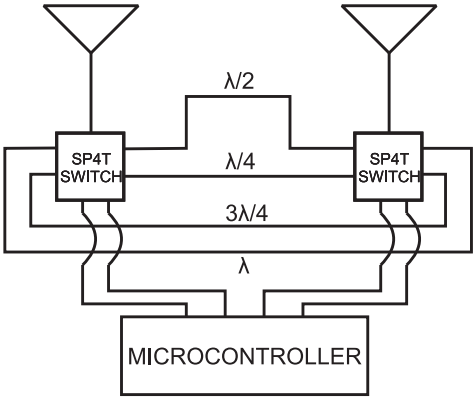

FIGURE 4. The circuit diagram of a retrodirective Van Atta array implementing QPSK modulation (©2012 IEEE [41]).

B. DELAY LINES

The second method for implementing high-order modulation is through adding delay lines. This method is common when implementing phase shift keying (PSK). However, this method is the least common method since the addition of delay lines increases—in general—the physical dimensions of the tag. Nonetheless, successful implementation of delay lines appeared in the literature. For instance, 4-QAM at 5.8 GHz [39], [40] and QPSK at 5.8 GHz [41]. To shed some light on the details of the aforementioned designs, the work of Trotter et al. [41] used a Van Atta array (more information on this type of arrays [42], [43], [44]) with two single pole four throw (SP4T) switches that switch between four distinct microstrip lines, which differ in length by a quarter wavelength ($\lambda/4$) as shown in Figure 4. The $\lambda/4$ difference between the lines translates to a 90° phase difference between adjacent symbols, which resemble—if plotted on the complex plane—a QPSK constellation.

A novel implementation of high order-modulation incorporating delay lines appeared recently in the work of Meng et al. [45] in which a four-element Van Atta retrodirective array is used to increase the backscatter range as well to implement QPSK modulation. In the design of [45]—shown in Figure 5—the outer antennas are reserved for phase-quadrature data while the inner antennas are dedicated to the in-phase data. At any instant, the phase different between the two pair of antennas is ±90°. In the design of [45], baseband data are mixed with IF frequency and used to control the phase of the array. The IF data are designed such that the only one side band spectrum is used. The latest design by the same group replaced the delay lines by lumped elements [46] in which a steerable beam can be generated.

C. SOLID-STATE DEVICES

One of the common methods for implementing high-order modulation is through the change in the impedance of a

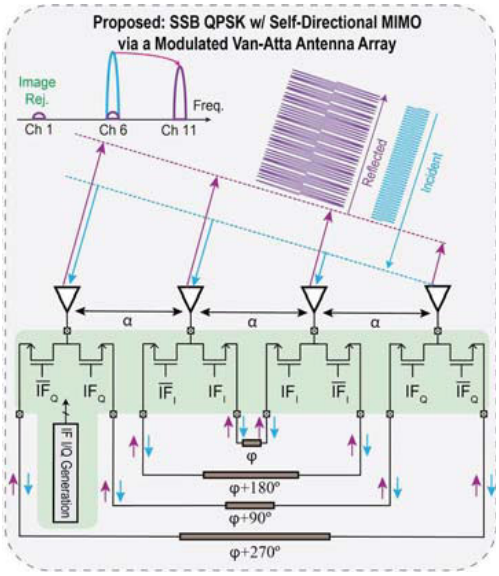

FIGURE 5. A four-element retrodirective array in [45] (© IEEE 2021 [45]).

FIGURE 6. The backscatter modulator in [47] in which V_1 through V_4 are the biasing voltages for the four MOSFET devices (© IEEE 2016 [47]).

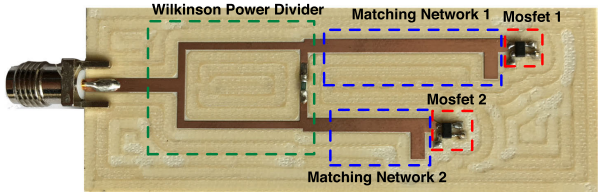

FIGURE 7. The backscatter modulator in [48] with an added Wilkinson power divider.(© IEEE 2017 [48]).

solid-state device (diode and/or transistor) in response to a biasing voltage. This technique is versatile, integratable, and flexible.

1) GENERAL WORK

Using a transistor-based implantation, Correia and Carvalho [47] presented a 4-QAM backscatter modulator operating at 2.45 GHz by connecting the tag antenna to four branches each of which is terminated with a MOSFET as shown in Figure 6. The change in the gate voltage between 0 and 0.6 V results in specific points in the constellation diagram. Each point represents a case in which one transistor is active and the remaining three are inactive. A key limitation in the design of [47] is that increasing the modulation order results in an increase in the number of transistors. In other words, the relationship between the number of transistors and the modulation order is 1-to-1. To overcome this issue, a later work by the same group [48] showed the possibility of designing a 16-QAM backscatter modulator using a Wilkinson power divider as shown in Figure 7. The power divider has a branch that is delayed by 45° compared to the other, which creates a round-trip phase delay of 90°. Compared to the design in [47], the design in [48] use intermediate values of the gate voltage to create different impedance levels, which result in different complex modulation levels. The authors were able to achieve a bit rate of 120 Mbps with an EVM of 16.7% and an energy efficiency of 6.7 pJ/bit. Reducing the bit rate to 60 Mbps results in an EVM of 10.3% with an energy efficiency of 16.7 pJ/bit.

An improvement to the system in [48] by the same authors appeared in [49] in which an energy harvester is optimized at 1.7 GHz (backscatter communications take place at 2.45 GHz). At the reader, an equalizer is used to achieve an energy efficiency of 61.5 fJ/bit using a 16-QAM modulator at a bit rate of 960 Mbps with a power consumption of 59μW. Going along the line of dual-frequency implementation, Correia and Carvalho [50] designed a dual-band backscatter modulator using a dual-band Wilkinson power divider that operates at 900 MHz and 2.45 GHz. The dual-band tag implements a 4-QAM modulation scheme and achieves an energy efficiency of 54 fJ/bit. The same research group also implemented a mm-wave (at 24 GHz) QAM modulator using 130-nm BiCMOS technology [51]. In their design, the authors implemented 16-, 32-, and 64-QAM modulation schemes.

One the earliest implementations of high-order modulation is through the combination power division and PIN diodes, which appeared in the work of Winkler et al. [52] as a modulator for UHF-based RFID tag emulator. In their design, the power division is achieved using a two-way Wilkinson power divider. The outputs of the divider feed a low-pass filter—in one branch—and a high-pass filter in the other branch. These two filters are 45° out of phase and the terminals of these filters are connected, separately, to PIN diodes as shown in Figure 8. The current of the diodes are controlled by the I and Q data. For testing purpose as well, Muralter et al. [53] proposed a computational UHF RFID platform compatible with commodity software-defined radio (SDR) in which the backscatter modulator consists of a dual-gate MOSFET. Each gate voltage is controlled by an independent stream of data, which yields three distinguishable reflection states.

Besides the aforementioned designs, several designs exist that are a mixture of two or more approaches. One of which is that proposed by Reed et al. [54] who used a combination of transistors (GaN HEMT) and varactor diodes to implement 16-QAM. The transistor controls the real part of reflection coefficient while the varactor diode controls the reactive part of the reflection coefficient.

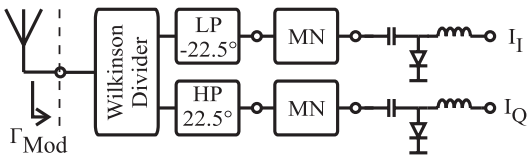

FIGURE 8. A circuit diagram of the QAM modulator in [52] (© IEEE 2010 [52]).

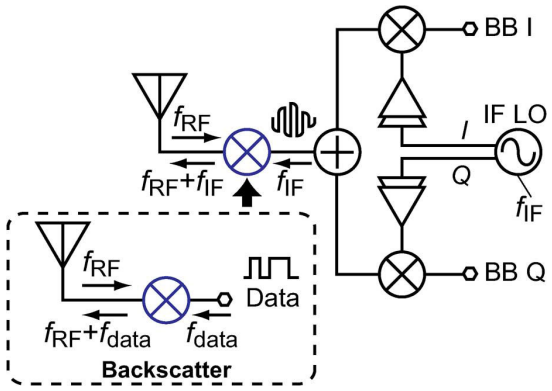

FIGURE 9. The circuit diagram of backscatter tag with an IF mixer in [55] (© IEEE 2015 [55]).

2) IF MIXING

A key feature of passive and semi-passive backscatter transponders is their low-power consumption. This criterion is accomplished through the avoidance of having radio transmitters on the tag. To go beyond what a standard system can achieve, some researchers implemented high-order modulation while maintaining a low power consumption by having an active source that is used purely for mixing at an intermediate frequency. For instance, Shirane et al. [55] designed a backscatter tag with a transceiver and a power management unit operating at a carrier frequency of 5.8 GHz. The tag has asymmetrical uplink and downlink. The downlink modulation is OOK while that for the uplink is 32-QAM. To reach such a high-order modulation while consuming minimal power, an intermediate frequency (IF) quadrature modulator operating at 96 MHz is used as shown in Figure 9. The power consumption of the tag is 133μW and the achieved energy efficiency is 45.2 pJ/bit. A recent design by Ide et al. [56] added a beamforming capability to the IF-backscatter system. Furthermore, IF backscatter mixing can be used as a 5G relay [57], which is beyond what standard backscatter systems can do.

Mixing an IF frequency with mm-wave frequency can also facilitate high-order modulation at mm-wave frequencies. For example, Kimionis et al. [58] designed a 24.5 GHz backscatter modulator on a flexible substrate. The authors tested BPSK, QPSK, and 16-QAM modulation schemes. For BPSK and QPSK, the data rate was set to 1 Gbps and the IF subscarrier operates at 2 GHz. However, for the 16-QAM, the data rate is increased to 2 Gbps. In this case, the system achieves an energy efficiency of 0.17 pJ/bit with a BER of 8% and an EVM of 12.37%.

3) APPLICATIONS

As in the case of lumped-element-based modulators, ambient backscatter communication is one of the applications that benefit from using a transistor-based, high-order, and variable impedance modulator. In the literature, several implementations of transistor-based backscatter modulators were targeting the increase in data throughput of ambient backscatter systems. For instance, Daskalakis et al. [59], [60] designed a 4-PAM backscatter modulator operating at the FM frequency band (87.5-108 MHz). The modulator comprises a sensor, a microcontroller, a 5-bit digital to analog converter (DAC). The sensing data feed the microcontroller, which in turn passes the data to the DAC, which controls the gate-voltage level. The system in [59] and [60] achieves a bit rate of 345 bps with an energy efficiency of 78.2 nJ/bit.[6]

The solid-state based backscatter system can be extended to acoustic communications. For instance, Christensen et al. [61] designed an ultrasound backscatter system for brain implants. The system implements a 4-ASK scheme achieving a date rate of 280 kbps.

4) ADVANCED TECHNIQUES & CONSIDERATIONS

A backscatter transponder is required to communicate its identity with the interrogator. If the transponder is connected to a sensor, the sensing data are communicated too. In order to simultaneously communicate the two types of information, a novel technique called piggyback modulation is proposed by Chen et al. [62], [63]. In their proposed design (shown in Figure 10), simultaneous identification and sensing of backscattered signals is achieved by varying the antenna impedance in response to the sensor data along with the impedance of the RFID application-specific integrated circuit (ASIC). The simultaneous change in the two impedances results in a four states as shown in the constellation plot of Figure 10. The variation of the antenna impedance is done through the use of a coupling loop. Since the constellation in Figure 10 does not lend itself into a well-known modulation, an advanced demodulation technique is needed. The authors in [63] experimented with 4-ASK and quasi 4-QAM demodulation techniques. The experiment showed that the quasi 4-QAM demodulation is the superior technique. Piggyback modulation is a powerful approach to tap into existing infrastructure, which results in a rather agile system.

Nonuniform modulation appeared also in the work of Ebrahimi-Asl et al. [64] in which a dual-loaded bowtie antenna is used to implement a quasi 32-QAM. Along the line of non-conventional (and nonuniform) modulation, Thomas and Howe [65] showed that by using an input/output pin in an off-shelf general-purpose microcontroller, 32 different states

[6]The authors in [60] also discussed the use of 10.2 kbps, which achieves an energy efficiency of 27.7 nJ/bit.

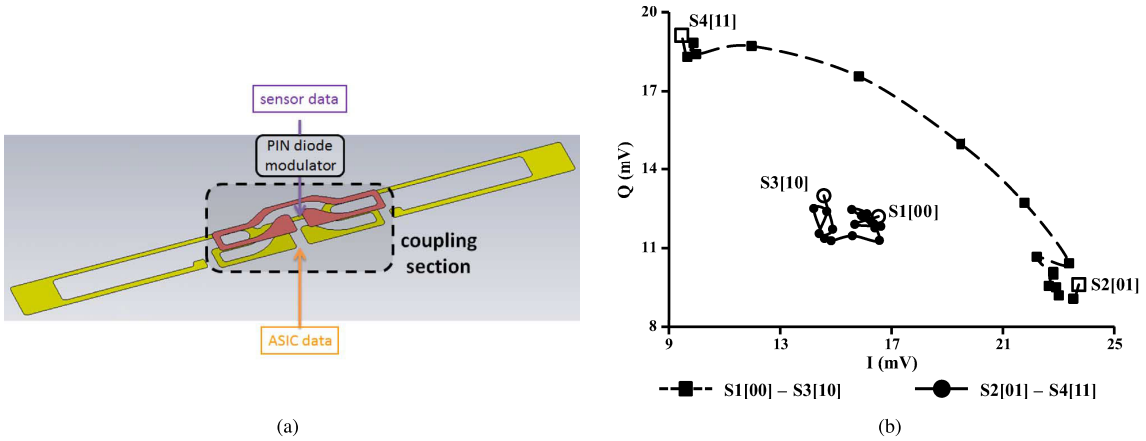

FIGURE 10. The piggyback modulator of [63]. (a) Circuit design. (b) Signal constellation. (© 2011 IEEE [63]).

per pin[7] can be implemented. These 32 states result in a four nonuniform clusters of points in the complex Γ plane yielding a quasi 4-QAM modulation scheme. Another design using a similar approach appeared in the work of Vision et al. [67] in which two general-purpose input/output (GPIO) pins of a PIC microcontroller are connected directly to the two arms of a dipole antenna. The design in [67] implements a 4-QAM modulation scheme. In fact, the designs in [65] and [67] show that high-order modulation can be implemented simply by using commercial off-the-shelf components, which significantly simplifies the design.

Going beyond 4-QAM, one of the overlooked issues related to high-order modulation is the constellation shape. In their recent work, Matos et al. [68] compared the performance of 16-QAM backscatter modulators with different constellation shapes operating at 2.45 GHz in terms of power consumption and symbol error rate (SER). The authors compared star-, hexagonal-, square-, and rectangular-QAM and concluded that for an SNR from 0 to 6 dB, all but rectangular-QAM perform approximately the same. However, for an SNR greater than 6 dB, Star-QAM outperforms the others and the performance gap—in terms of SER—increases with the increase in SNR.

D. SUMMARY AND CONCLUDING REMARKS

To summarize the work done in the field of high-order modulation, Table 2 lists some of the exemplary designs covered in this section along with their specifications. For the sake of brevity, the related designs—which by themselves are significant—are listed too.

IV. SINGLE SIDEBAND (SSB) MODULATION

One of the challenging problems that hinders the co-existence of backscatter systems with other wireless standards is the interference caused by adjacent channels. The problem becomes more pronounced when one sideband of the spectrum does not experience strong interference while the other does. In such a situation, half of the signal energy is being compromised. Another issue that might arise in such a case is when the channels of both sidebands are the only available channels for transmission with minimal interference. In both scenarios, using SSB modulation would increase the spectral efficiency.

For SSB modulation, the passband signal can be written as [19] and [69]

$$s_{\text{SSB}}(t) = g(t)\cos(2\pi f_c t) \pm \hat{g}(t)\sin(2\pi f_c t), \tag{9}$$

where $g(t)$ is the baseband pulse and $\hat{g}(t)$ is the Hilbert transform of $g(t)$. The plus and minus signs correspond to the lower and upper sidebands, respectively. Equation (9) resembles a special case of 4-QAM; however, in general, SSB transmits the *same* stream of data through two channels while QAM transmits two streams of data over two channels. The distinction between them becomes clearer when writing their complex passband representation. That is [19],

$$s_{\text{SSB}}(t) = \Re\{A_m \left[g(t) \pm j\hat{g}(t)\right] \exp(j2\pi f_c t)\}, \tag{10}$$

where $m = 1, 2, \ldots M$ and M is the size of the alphabet. On the other hand, QAM modulation can be written as [19]

$$s_{\text{QAM}}(t) = \Re\{(A_{mi} + jA_{mq})g(t)e^{j2\pi f_c t}\}, \tag{11}$$

where A_{mi} and A_{mq} are the two independent streams of data in in-phase and quadrature channels, respectively.

A. EXISTING WORK

The work on SSB backscatter modulation is rather recent compared to both high-order modulation and pulse shaping. It is, however, motivated by the co-existence of the RFID technology with other wireless communications technologies.

[7]The 32 states are specific to the off-the-shelf microcontroller, which is [66].

TABLE 2. Summary and key features of the work in high-order backscatter modulation systems.

Reference	Frequency	Modulation Type	Implementation Topology	Data Rate	Power Consumption	Energy Efficiency	EVM	Range	Related Work
[23]	915 MHz	16-QAM	Lumped elements	96 Mbps	1.49 mW	15.5 pJ/bit	9.38%	3.8λ	[16], [21], [24], [25], [29], [31], [38]
[26]	2.4 GHz	16-QAM	On chip	100 Mbps	25 μW	0.25 pJ/bit	9.078%	Cabled	-
[35]	909 MHz	DQPSK	Lumped elements	25 Mbps	309 μW	12.4 pJ/bit	9.7%	1.1λ	[34], [36], [37], [69], [70]
[41]	5.8 GHz	QPSK	Delay lines	2 Mbps	-	-	-	12λ	[39], [40], [45], [46]
[63]	915 MHz	Quasi 4-QAM	Lumped elements	10 kbps	-	-	-	-	[62], [64], [65]
[55]	5.8 GHz	32-QAM	On chip (IF modulation)	2.5 Mbps	113 μW	45.2 pJ/bit	4.6%	1.92λ	[30], [56], [57]
[49]	2.45 GHz	16-QAM	FET with variable gate voltage	960 Mbps	59 μW	61.5 fJ/bit	8.37%	Cabled	[47], [48], [50], [51]
[58]	24.5 GHz	16-QAM	Transistor (E-pHEMT)	2 Gbps	1.36 mW	0.17 pJ/bit	12.37%	40.4λ	-
[60]	98.5 MHz (FM range)	4-PAM	Transistor (E-pHEMT)	345 bps	27μ W	78.2 nJ/bit	-	0.5λ	[59]

Notes:
- Reported results are for the fastest data rate in the reference.
- Reported results are also for the highest modulation order in the reference.
- Some of the results are not stated in the reference but rather inferred from other results within that reference.

One of the earliest designs in the literature appeared in the work of Rosenthal and Reynolds [69] who studied the co-existence of backscatter communications with BLE technology. In their work, the generation of the Hilbert transform of the signal can be achieved by noticing that the Hilbert transform of baseband square pulse is equivalent to delaying the pulse by a quarter period as shown in Figure 11. Therefore, we have two *dependent* streams of data. These two streams control an SP4T switch that switches between four distinct impedances. Referring to Figure 11, the key difference between 4-QAM and the BPSK SSB (the one used in [69]) is depicted in the state machine. In the latter, a transition to the same state is not permissible while in the former, we can have transition to the same state. The design in [69] yields a sideband suppression of 10 dB while having a spectral efficiency of 198 pJ/bit. An improvement to this design is presented by the same authors [70] in which inductors are replaced by CMOS digitally-tuned capacitors (DTC) for better integration. The same authors also used SSB to implement an all digital OFDM backscatter modulator [71], [72] with five subcarriers achieving a data rate of 1.25 Mbps with a spectral efficiency of 160 pJ/bit. In [72], delta-sigma modulation block is added to the tag before the digital to analog converter (DAC) (i.e., an RF switch) to reduce the quantization noise around the subcarriers.

In some of the designs available in the literature, a combination of high-order modulation and SSB modulation is used to simultaneously increase the spectral efficiency while reducing the interference from the image. For example, Wang et al. [30] achieved a sideband image rejection of 17 dB. Another design appeared in the work Meng et al. [45] in which an image rejection of 18 dB is achieved.

V. PULSE SHAPING

Most of backscatter modulators are based on square pulses. The rationale behind that is the stringent requirements for minimizing the on-tag power consumption. Despite this, some proof-of-concept designs exist in the literature.

A. THE NEED FOR PULSE SHAPING

Backscatter systems operate in a congested spectrum and naturally, a low-powered communication. Such a requirement become problematic[8] in the microwave and millimeter-wave (mm-wave) frequencies in which these systems need to co-exist with other local area network (LAN) standards. Therefore, out-of band emission needs to be reduced. The textbook approach from a waveform perspective is to change the nature of the baseband waveform.

Since out-of-band energy is wasted, an important metric to consider is the energy efficiency, which is defined differently from the one in (8). In fact, the definition given in (8) looks into the efficiency from the tag perceptive. In other words, the efficiency in (8) assumes all emitted energy are captured

[8]Some nonlinearity effect such as those in [73] and [74] becomes significant.

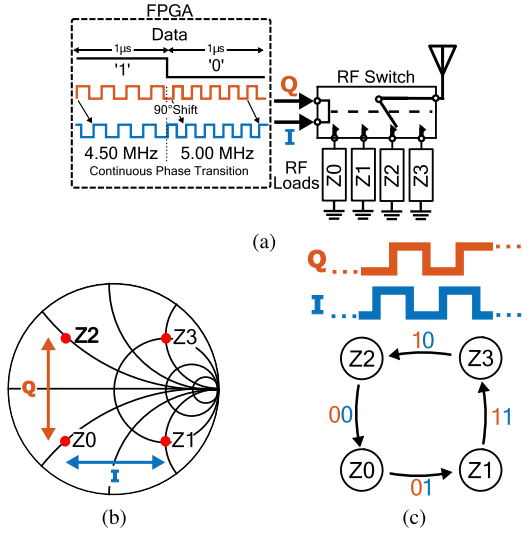

FIGURE 11. The structure of the SSB modulator in [69]. (a) Circuit topology. (b) Smith chart representation of ideal impedances. (c) State machine representation for the impedance switching. © IEEE 2019 [69].

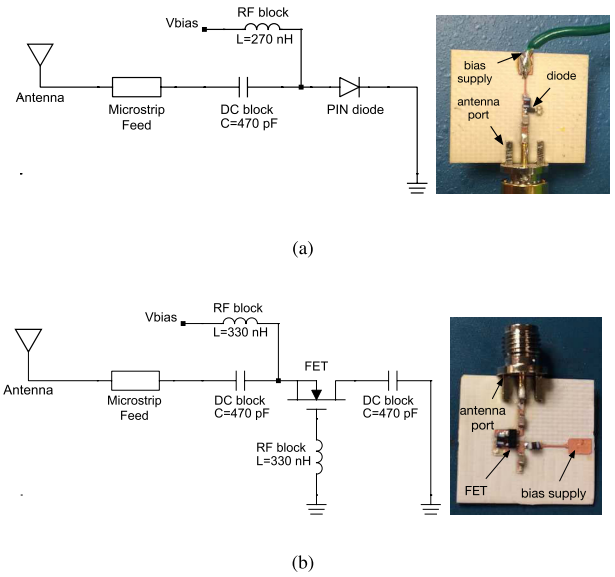

FIGURE 12. PIN diode (a) and FET (b) implementations of a pulse-shaping transponder (© IEEE 2016 [75]).

by the reader. In practise, the reader and the channel are both bandlimited, which implies that only radiated energy within the bandwidth of the system is *actually* contributing to the data communication. In such a case, the energy efficiency could be defined as follows [75]

$$\text{Actual Energy Efficiency} = \text{Energy Efficiency} \cdot L_{\text{BW}}, \tag{12}$$

where the first term in the right-hand side is the efficiency in (8) and L_{BW} is the bandwidth loss (unitless) and is defined as [75]

$$L_{\text{BW}} = \frac{\text{In-band Energy}}{\text{Total Energy}}. \tag{13}$$

B. EXISTING WORK

The backscatter literature is not rich in this area as a result of the complexity added to the tag, which must be averted. Nevertheless, few *exemplary* designs have promising results. For instance, Kimionis and Tentzeris [75] developed a systematic approach to synthesize different pulses and experimentally validated their approach using a square root raised cosine (SRRC) pulse. In their design, pulse shaping can be generated using either a PIN diode or an FET, both approaches are shown in Figure 12. To synthesize the desired pulse, the authors established a functional mapping between the reflection coefficient of the modulator and the biasing voltage of the diode or the FET. The authors also investigated the use of both binary modulation and 4-PAM. In addition, pulse shaping can be used to implement high-order modulation at mm-wave frequencies [58].

In the microwave frequencies, Tang et al. [76] designed an integrated circuit implementing a transmit pulse shaping along with symbol pre-distortion operating at a frequency

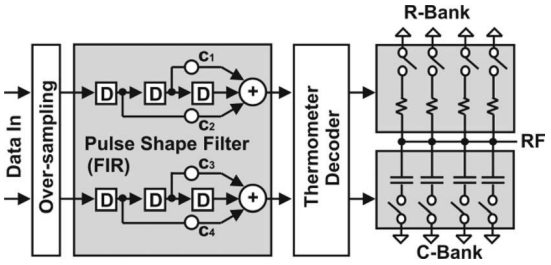

FIGURE 13. A 5.8 GHz transponder with pulse shaping (© IEEE 2016 [76]).

of 5.8 GHz and transmitting at a rate of 54 Mbps. Pulse shaping is implemented by oversampling the data signals that feed the R and C discrete impedance banks as shown in Figure 13. The oversampled data are then passed to a finite impulse response (FIR) filter whose coefficients are optimized to reduce the adjacent channel power ratio (ACPR). The smooth transition between impedance states reduces the out-of-band emission and hence reduces ACPR making the backscatter system compatible with the requirements of the IEEE 802.11 standard. In addition, symbol pre-distortion is achieved by having more states than needed—the modulation requires only four states since it is QPSK—and the states are manually optimized to reduce the EVM.

Another promising work appeared in [77] in which a Gaussian pulse-shaping was synthesized using FET with different gate voltages. The design uses voltage divider network with control signals that create different sets of the voltage levels. The generated discrete levels translate to quantized pulses that are more feasible to generate in a low-powered devices compared to continuous pulses. Experimentally, the reported adjacent channel power ratio is 7.5 dBc.

VI. CONCLUSION AND FUTURE DIRECTIONS

In this article, a summary of existing designs that target increasing the spectral efficiency of backscatter system—with proven prototypes—is presented. As shown in this article, three techniques are common to increase the efficiency, which are: high-order modulation, SSB modulation, and pulse shaping. Among these three techniques, high-order modulation is the mature one with a plethora of designs while the last two are less common. On the other hand, using either SSB or pulse-shaping techniques may result in an increase the device complexity and physical size, which in turns increases the cost of implementing these techniques compared to their high-order modulation counterpart.

Looking into the literature, advancements in wireless technologies, and future of connectivity; co-existence with other wireless standards is very critical, which requires significant work on a less-investigated areas of SSB modulation and pulse shaping. In fact, several concerns are needed to be addressed. These concerns are: optimal pulse shaping, role of artificial intelligence (AI), multi-carrier modulation, and agile modulators.

A. OPTIMAL PULSE SHAPING

Although the literature has designs that implement pulse shaping. An unanswered question is what is the optimal pulse shaping? In fact, the nature of backscatter communications imposes several limitations in terms of power consumption, synthesis of the required pulse, and spectral efficiency. Using the quantization method in [77], we can synthesize any pulse but some *might* be easier to implement than others. Another point to consider is the location of pulse shaping filter, would it be more efficient if it is moved to the interrogator? These open-ended problems can be a research direction for future co-existence of backscatter communications with other standards.

B. ARTIFICIAL INTELLIGENCE

One of the applications of AI in physical-layer communications in for modulation classification [78], [79]. using AI-assisted classification, high-order modulation can be detected at the receiver even with moderate or low SNR. A more optimistic approach is design an end-to-end communication system in which modulation and demodulation are performed with the aid of AI.

C. MULTI-CARRIER MODULATION

One of the techniques that shaped the wireless communications technologies in recent years is the use of OFDM. In the backscatter literature, few designs have explored OFDM or OFDM-like modulation such as [71], [72], and [80]. In fact, multi-carrier modulation offers a compromise between double-fading nature of backscatter channels [10], low-power consumption constraint, fast data rate, and system complexity.

D. AGILE MODULATION

In some situations, the SNR is low, which requires reducing the data rate to increase the reliability of the communication link. In other cases, however, the SNR is high but the data rate is low since the system is designed for the worst case scenario. Therefore, a universal backscatter modulator is needed. One solution is at the stage when the communication channel between the tag and reader is established, the latter can estimate the SNR and instruct the former to use a specific modulation scheme. A feasibility study, power budget calculations, and communication protocol are topics that require further investigation before implementing such a system.

ACKNOWLEDGMENT

The author would like to thank Prof. Ali H. Muqaibel for his valuable comments during the manuscript preparation.

REFERENCES

[1] H. Stockman, "Communication by means of reflected power," *Proc. IRE*, vol. 36, no. 10, pp. 1196–1204, Oct. 1948.
[2] S. F. Wamba, A. Anand, and L. Carter, "A literature review of RFID-enabled healthcare applications and issues," *Int. J. Inf. Manage.*, vol. 33, no. 5, pp. 875–891, Oct. 2013.
[3] M. Yamin and Y. Ades, "Crowd management with RFID and wireless technologies," in *Proc. 1st Int. Conf. Netw. Commun.*, 2009, pp. 439–442.
[4] A. Nasir, B. H. Soong, and K. A. Qaraqe, "RFID in-pipe moisture sensing system for oil and gas quality monitoring in Qatar," in *Proc. 19th IEEE Int. Conf. Netw. (ICON)*, Dec. 2013, pp. 1–5.
[5] GS1. *EPC^{TM} Radio-Frequency Identity Protocols Generation-2 UHF RFID Standard*. Accessed: Sep. 19, 2022. [Online]. Available: https://www.gs1.org/standards/rfid/uhf-airinterface-protocol
[6] *Information Technology—Radio Frequency Identification for Item Management—Part 63: Parameters for Air Interface Communications at 860 MHz to 960 MHz Type C*, Standard ISO/IEC 18000-63:2021, 2021. [Online]. Available: https://www.iso.org/standard/78309.html
[7] IEEE RFID. (2020). *Workshop: What Should Gen3 be?*. [Online]. Available: https://2020.ieee-rfid.org/workshop-on-what-should-gen3-be/
[8] J. D. Griffin and G. D. Durgin, "Link envelope correlation in the backscatter channel," *IEEE Commun. Lett.*, vol. 11, no. 9, pp. 735–737, Sep. 2007.
[9] D. Arnitz, U. Muehlmann, and K. Witrisal, "Wideband characterization of backscatter channels: Derivations and theoretical background," *IEEE Trans. Antennas Propag.*, vol. 60, no. 1, pp. 257–266, Jan. 2012.
[10] M. Alhassoun and G. D. Durgin, "Spatial fading in backscatter channels: Theory and models," in *Proc. 16th IEEE Annu. Consum. Commun. Netw. Conf. (CCNC)*, Jan. 2019, pp. 1–6.
[11] G. D. Durgin and B. P. Degnan, "A better channel code than FM0 for next-generation RFID," in *Proc. IEEE Int. Conf. RFID (RFID)*, May 2017, pp. 1–5.
[12] J. R. Barry, E. A. Lee, and D. G. Messerschmitt, *Digital Communication*. Cham, Switzerland: Springer, 2012.
[13] P. V. Nikitin, K. V. S. Rao, and R. D. Martinez, "Differential RCS of RFID tag," *Electron. Lett.*, vol. 43, no. 8, p. 431, 2007.
[14] F. Fuschini, C. Piersanti, F. Paolazzi, and G. Falciasecca, "Analytical approach to the backscattering from UHF RFID transponder," *IEEE Antenna Wireless Propag. Lett.*, vol. 7, pp. 33–35, 2008.
[15] G. D. Durgin, C. R. Valenta, M. B. Akbar, M. M. Morys, B. R. Marshall, and Y. Lu, "Modulation and sensitivity limits for backscatter receivers," in *Proc. IEEE Int. Conf. RFID (RFID)*, Apr. 2013, pp. 124–130.
[16] S. Thomas and M. S. Reynolds, "QAM backscatter for passive UHF RFID tags," in *Proc. IEEE Int. Conf. RFID* , Apr. 2010, pp. 210–214.
[17] K. M. Gharaibeh, K. G. Gard, and M. B. Steer, "Accurate estimation of digital communication system metrics—SNR, EVM and ρ in a nonlinear amplifier environment," in *Proc. 64th ARFTG Microw. Meas. Conf.*, Dec. 2004, pp. 41–44.
[18] R. A. Shafik, M. S. Rahman, and A. R. Islam, "On the extended relationships among EVM, BER and SNR as performance metrics," in *Proc. Int. Conf. Electr. Comput. Eng.*, Dec. 2006, pp. 408–411.

[19] J. Proakis and M. Salehi, *Digital Communications. Great Britain*, 5th ed. New York, NY, USA: McGraw-Hill, 2014.

[20] E. Bjornson and E. G. Larsson, "How energy-efficient can a wireless communication system become?" in *Proc. 52nd Asilomar Conf. Signals, Syst., Comput.*, Oct. 2018, pp. 1252–1256.

[21] S. J. Thomas, E. Wheeler, J. Teizer, and M. S. Reynolds, "Quadrature amplitude modulated backscatter in passive and semipassive UHF RFID systems," *IEEE Trans. Microw. Theory Techn.*, vol. 60, no. 4, pp. 1175–1182, Apr. 2012.

[22] R. B. Green, "The general theory of antenna scattering," Ph.D. dissertation, Dept. Elect. Eng., Ohio State Univ., Columbus, OH, USA, 1963.

[23] S. J. Thomas and M. S. Reynolds, "A 96 Mbit/sec, 15.5 pJ/bit 16-QAM modulator for UHF backscatter communication," in *Proc. IEEE Int. Conf. RFID (RFID)*, Apr. 2012, pp. 185–190.

[24] J. Besnoff and D. Ricketts, "Quadrature amplitude modulated (QAM) communication link for near and mid-range RFID systems," in *Proc. IEEE Int. Conf. RFID (RFID)*, Apr. 2015, pp. 151–157.

[25] J. Besnoff, M. Abbasi, and D. S. Ricketts, "High data-rate communication in near-field RFID and wireless power using higher order modulation," *IEEE Trans. Microw. Theory Techn.*, vol. 64, no. 2, pp. 401–413, Feb. 2016.

[26] E. Gong, H. Zhang, X. Chen, L. Ye, and R. Huang, "2.4-GHz 16-QAM passive backscatter transmitter for wireless self-power chips in IoT," in *Proc. IEEE Int. Symp. Circuits Syst. (ISCAS)*, Oct. 2020, pp. 1–5.

[27] V. Liu, A. Parks, V. Talla, S. Gollakota, D. Wetherall, and J. R. Smith, "Ambient backscatter: Wireless communication out of thin air," *ACM SIGCOMM Comput. Commun. Rev.*, vol. 43, no. 4, pp. 39–50, Oct. 2013.

[28] A. Wang, V. Iyer, V. Talla, J. R. Smith, and S. Gollakota, "FM backscatter: Enabling connected cities and smart fabrics," in *Proc. 14th USENIX Symp. Networked Syst. Design Implement.*, 2017, pp. 243–258.

[29] Y.-H. Kim, C. Yoon, H.-S. Ahn, and S.-O. Lim, "Implementation of multi-level modulated-backscatter communication system using ambient Wi-Fi signal," in *Proc. IEEE Int. Conf. RFID Technol. Appl. (RFID-TA)*, Sep. 2019, pp. 476–479.

[30] P.-H.-P. Wang, C. Zhang, H. Yang, M. Dunna, D. Bharadia, and P. P. Mercier, "A low-power backscatter modulation system communicating across tens of meters with standards-compliant Wi-Fi transceivers," *IEEE J. Solid-State Circuits*, vol. 55, no. 11, pp. 2959–2969, Nov. 2020.

[31] J. Qian, A. N. Parks, J. R. Smith, F. Gao, and S. Jin, "IoT communications with M-PSK modulated ambient backscatter: Algorithm, analysis, and implementation," *IEEE Internet Things J.*, vol. 6, no. 1, pp. 844–855, Feb. 2019.

[32] J. Zhao, W. Gong, and J. Liu, "Spatial stream backscatter using commodity WiFi," in *Proc. 16th Annu. Int. Conf. Mobile Syst., Appl., Services*, 2018, pp. 191–203.

[33] Y. Yang and W. Gong, "Universal space-time stream backscatter with ambient WiFi," in *Proc. IEEE Int. Conf. Pervasive Comput. Commun. (PerCom)*, Mar. 2022, pp. 101–110.

[34] J. Rosenthal, E. Kampianakis, A. Sharma, and M. S. Reynolds, "A 6.25 Mbps, 12.4 pJ/bit DQPSK backscatter wireless uplink for the NeuroDisc brain–computer interface," in *Proc. IEEE Biomed. Circuits Syst. Conf. (BioCAS)*, Oct. 2018, pp. 1–4.

[35] J. Rosenthal, A. Sharma, E. Kampianakis, and M. S. Reynolds, "A 25 Mbps, 12.4 pJ/b DQPSK backscatter data uplink for the NeuroDisc brain–computer interface," *IEEE Trans. Biomed. Circuits Syst.*, vol. 13, no. 5, pp. 858–867, Oct. 2019.

[36] A. Sharma, E. Kampianakis, J. Rosenthal, A. Pike, A. Dadkhah, and M. S. Reynolds, "Wideband UHF DQPSK backscatter communication in reverberant cavity animal cage environments," *IEEE Trans. Antennas Propag.*, vol. 67, no. 8, pp. 5002–5011, Aug. 2019.

[37] J. Rosenthal and M. S. Reynolds, "A dual-band shared-hardware 900 Mhz 6.25 Mbps DQPSK and 2.4 GHz 1.0 Mbps Bluetooth low energy (BLE) backscatter uplink for wireless brain–computer interfaces," in *Proc. IEEE Int. Conf. RFID (RFID)*, Sep. 2020, pp. 1–6.

[38] S. S. Afzal, R. Ghaffarivardavagh, W. Akbar, O. Rodriguez, and F. Adib, "Enabling higher-order modulation for underwater backscatter communication," in *Proc. Global Oceans*, Oct. 2020, pp. 1–6.

[39] E. Denicke, D. Härke, and B. Geck, "Investigating multi-antenna RFID systems by means of time-varying scattering parameters," in *Proc. 7th Eur. Conf. Antennas Propag. (EuCAP)*, Apr. 2013, pp. 3314–3318.

[40] E. Denicke, H. Hartmann, B. Geck, and D. Manteuffel, "MIMO backscatter channel and data transmission measurements," in *Proc. 47th Eur. Microw. Conf. (EuMC)*, Oct. 2017, pp. 723–726.

[41] M. S. Trotter, C. R. Valenta, G. A. Koo, B. R. Marshall, and G. D. Durgin, "Multi-antenna techniques for enabling passive RFID tags and sensors at microwave frequencies," in *Proc. IEEE Int. Conf. RFID (RFID)*, Apr. 2012, pp. 1–7.

[42] L. C. Van Atta, "Electromagnetic reflector," U.S. Patent 2 908 002, 1959.

[43] C. Y. Pon, "Retrodirective array using the heterodyne technique," *IEEE Trans. Antennas Propag.*, vol. AP-12, no. 2, pp. 176–180, Mar. 1964.

[44] E. Sharp and M. Diab, "Van Atta reflector array," *IRE Trans. Antennas Propag.*, vol. 8, no. 4, pp. 436–438, Jul. 1960.

[45] M. Meng, M. Dunna, H. Yu, S. Kuo, P.-H.-P. Wang, D. Bharadia, and P. P. Mercier, "12.2 improving the range of WiFi backscatter via a passive retro-reflective single-side-band-modulating MIMO array and non-absorbing termination," in *IEEE Int. Solid-State Circuits Conf. (ISSCC) Dig. Tech. Papers*, Feb. 2021, pp. 202–204.

[46] S.-K. Kuo, M. Dunna, D. Bharadia, and P. P. Mercier, "A WiFi and Bluetooth backscattering combo chip featuring beam steering via a fully-reflective phased-controlled multi-antenna termination technique enabling operation over 56 meters," in *IEEE Int. Solid-State Circuits Conf. (ISSCC) Dig. Tech. Papers*, Feb. 2022, pp. 1–3.

[47] R. Correia and N. B. Carvalho, "Design of high order modulation backscatter wireless sensor for passive IoT solutions," in *Proc. IEEE Wireless Power Transf. Conf. (WPTC)*, May 2016, pp. 1–3.

[48] R. Correia, A. Boaventura, and N. B. Carvalho, "Quadrature amplitude backscatter modulator for passive wireless sensors in IoT applications," *IEEE Trans. Microw. Theory Techn.*, vol. 65, no. 4, pp. 1103–1110, Apr. 2017.

[49] R. Correia and N. B. Carvalho, "Ultrafast backscatter modulator with low-power consumption and wireless power transmission capabilities," *IEEE Microw. Wireless Compon. Lett.*, vol. 27, no. 12, pp. 1152–1154, Dec. 2017.

[50] R. Correia and N. B. Carvalho, "Dual-band high order modulation ambient backscatter," in *IEEE MTT-S Int. Microw. Symp. Dig.*, Jun. 2018, pp. 270–273.

[51] D. Matos, M. D. da Cruz Jordao, R. Correia, and N. B. Carvalho, "Millimeter-wave BiCMOS backscatter modulator for 5G-IoT applications," *IEEE Microw. Wireless Compon. Lett.*, vol. 31, no. 2, pp. 173–176, Feb. 2021.

[52] M. Winkler, T. Faseth, H. Arthaber, and G. Magerl, "An UHF RFID tag emulator for precise emulation of the physical layer," in *Proc. 40th Eur. Microw. Conf.*, 2010, pp. 1750–1753.

[53] F. Muralter, L. Arjona, H. Landaluce, and A. Perallos, "A passive computational UHF RFID platform using vector backscatter modulation," *IEEE Sensors J.*, vol. 22, no. 6, pp. 6145–6149, Mar. 2022.

[54] R. Reed, F. L. Pour, and D. S. Ha, "An energy efficient RF backscatter modulator for IoT applications," in *Proc. IEEE Int. Symp. Circuits Syst. (ISCAS)*, May 2021, pp. 1–5.

[55] A. Shirane, Y. Fang, H. Tan, T. Ibe, H. Ito, N. Ishihara, and K. Masu, "RF-powered transceiver with an energy- and spectral-efficient IF-based quadrature backscattering transmitter," *IEEE J. Solid-State Circuits*, vol. 50, no. 12, pp. 2975–2987, Dec. 2015.

[56] M. Ide, A. Shirane, K. Yanagisawa, D. You, J. Pang, and K. Okada, "A 28-GHz phased-array relay transceiver for 5G network using vector-summing backscatter with 24-GHz wireless power and LO transfer," *IEEE J. Solid-State Circuits*, vol. 57, no. 4, pp. 1211–1223, Apr. 2022.

[57] M. Ide, A. Shirane, K. Yanagisawa, D. You, J. Pang, and K. Okada, "A 28-GHz phased-array relay transceiver for 5G network using vector-summing backscatter with 24-GHz wireless power and LO transfer," in *Proc. Symp. VLSI Circuits*, Jun. 2021, pp. 1–2.

[58] J. Kimionis, A. Georgiadis, S. N. Daskalakis, and M. M. Tentzeris, "A printed millimetre-wave modulator and antenna array for backscatter communications at gigabit data rates," *Nature Electron.*, vol. 4, no. 6, pp. 439–446, Jun. 2021.

[59] S. N. Daskalakis, R. Correia, G. Goussetis, M. M. Tentzeris, N. B. Carvalho, and A. Georgiadis, "Spectrally efficient 4-PAM ambient FM backscattering for wireless sensing and RFID applications," in *IEEE MTT-S Int. Microw. Symp. Dig.*, Jun. 2018, pp. 266–269.

[60] S. N. Daskalakis, R. Correia, G. Goussetis, M. M. Tentzeris, N. B. Carvalho, and A. Georgiadis, "Four-PAM modulation of ambient FM backscattering for spectrally efficient low-power applications," *IEEE Trans. Microw. Theory Techn.*, vol. 66, no. 12, pp. 5909–5921, Dec. 2018.

[61] M. N. Christensen, M. Zamani, A. Rashidi, and F. Moradi, "Ultrasonic backscatter communication for brain implants: Mathematical model, simulation, and measurement," in *Proc. IEEE Biomed. Circuits Syst. Conf. (BioCAS)*, Oct. 2021, pp. 1–5.
[62] H. Chen, A. Bhadkamkar, and D. W. van der Weide, "Piggyback modulation for UHF RFID sensors," in *IEEE MTT-S Int. Microw. Symp. Dig.*, May 2010, p. 1.
[63] H.-Y. Chen, A. S. Bhadkamkar, T.-H. Chou, and D. W. van der Weide, "Vector backscattered signals improve piggyback modulation for sensing with passive UHF RFID tags," *IEEE Trans. Microw. Theory Techn.*, vol. 59, no. 12, pp. 3538–3545, Dec. 2011.
[64] S. Ebrahimi-Asl, M. T. Ghasr, and M. J. Zawodniok, "Design of dual-loaded RFID tag for higher order modulations," *IEEE Trans. Microw. Theory Techn.*, vol. 66, no. 1, pp. 410–419, Jan. 2018.
[65] S. J. Thomas and J. A. Howe, "Achieving multistate vector scattering with unmodified digital input/output pins," *IEEE J. Radio Freq. Identificat.*, vol. 5, no. 3, pp. 311–316, Sep. 2021.
[66] Silicon Labs. *EFM8 Busy Bee Family EFM8BB1 Data Sheet*. Accessed: Jul. 18, 2022. [Online]. Available: https://www.silabs.com/documents/public/datasheets/efm8bb1-datasheet.pdf
[67] A. Voisin, A. Dumas, N. Barbot, and S. Tedjini, "Differential RCS of multi-state transponder," in *Proc. Wireless Power Week*, Jul. 2022, pp. 195–198.
[68] D. Matos, R. Correia, H. T. P. Silva, H. S. Silva, A. S. R. Oliveira, and N. B. Carvalho, "On the performance of square, rectangular, star, and hexagonal QAM for backscatter systems," *IEEE Microw. Wireless Compon. Lett.*, vol. 33, no. 1, pp. 102–105, Jan. 2023.
[69] J. Rosenthal and M. S. Reynolds, "A 1.0-Mb/s 198-pJ/bit Bluetooth low-energy compatible single sideband backscatter uplink for the NeuroDisc brain–computer interface," *IEEE Trans. Microw. Theory Techn.*, vol. 67, no. 10, pp. 4015–4022, Oct. 2019.
[70] J. Rosenthal and M. S. Reynolds, "All-digital single sideband (SSB) Bluetooth low energy (BLE) backscatter with an inductor-free, digitally-tuned capacitance modulator," in *IEEE MTT-S Int. Microw. Symp. Dig.*, Aug. 2020, pp. 468–471.
[71] J. D. Rosenthal and M. S. Reynolds, "Hardware-efficient all-digital architectures for OFDM backscatter modulators," *IEEE Trans. Microw. Theory Techn.*, vol. 69, no. 1, pp. 803–811, Jan. 2021.
[72] J. D. Rosenthal and M. S. Reynolds, "An all-digital 1.25 Mbps 5-subcarrier OFDM backscatter uplink with delta-sigma modulation for improved spurious-free dynamic range," in *Proc. IEEE Int. Conf. RFID (RFID)*, May 2022, pp. 103–108.
[73] D. M. Pozar, *Microwave Engineering*. Hoboken, NJ, USA: Wiley, 2011.
[74] B. Razavi and R. Behzad, *RF Microelectronics*, vol. 2. New York, NY, USA: Prentice-Hall, 2012.
[75] J. Kimionis and M. M. Tentzeris, "Pulse shaping: The missing piece of backscatter radio and RFID," *IEEE Trans. Microw. Theory Techn.*, vol. 64, no. 12, pp. 4774–4788, Dec. 2016.
[76] A. Tang, Y. Kim, Y. Xu, and M.-C. F. Chang, "A 5.8 GHz 54 Mb/s backscatter modulator for WLAN with symbol pre-distortion and transmit pulse shaping," *IEEE Microw. Wireless Compon. Lett.*, vol. 26, no. 9, pp. 729–731, Sep. 2016.
[77] M. Ferdik, G. Saxl, D. Gunjic, and T. Ussmueller, "Spectral efficiency increase for passive backscatter communication based on discrete pulse shaping," *IEEE Access*, vol. 6, pp. 50875–50881, 2018.
[78] T. O'Shea and J. Hoydis, "An introduction to deep learning for the physical layer," *IEEE Trans. Cogn. Commun. Netw.*, vol. 3, no. 4, pp. 563–575, Dec. 2017.
[79] T. Huynh-The, Q.-V. Pham, T.-V. Nguyen, T. T. Nguyen, R. Ruby, and M. Zeng, "Automatic modulation classification: A deep architecture survey," *IEEE Access*, vol. 9, pp. 142950–142971, 2021.
[80] R. Correia and N. B. Carvalho, "OFDM-like high order backscatter modulation," in *IEEE MTT-S Int. Microw. Symp. Dig.*, Aug. 2018, pp. 1–3.

MOHAMMAD ALHASSOUN (Member, IEEE) received the B.Sc. degree in electrical engineering from the King Fahd University of Petroleum and Minerals (KFUPM), Saudi Arabia, in 2013, and the M.S. and Ph.D. degrees from the Georgia Institute of Technology, Atlanta, in 2015 and 2019, respectively. He is currently an Assistant Professor with KFUPM. Previously, he worked at the Nokia Bell Laboratories as an EMCD Intern and a Graduate Assistant at KFUPM, where he was awarded the Best Laboratory Instructor at the Department of Electrical Engineering. He was also awarded the Tech to Teaching Certificate at the College Teaching, Georgia Institute of Technology, in addition to the Associate Level Certificate from the Center of Integration of Research, Teaching and Learning. His research interests include radio-channel modeling, retrodirective backscatter communications, spectrally-efficient backscatter systems, and physical-layer applications of machine learning. He was a recipient of both the 2018 and 2019 IEEE International Conference on RFID Best Paper Award.